

NASA Technical Memorandum 4729

# Dynamic Analysis With Stress Mode Animation by the Integrated Force Method

Surya N. Patnaik, Rula M. Coroneos, and Dale A. Hopkins

April 1997



National Aeronautics and  
Space Administration

NASA Technical Memorandum 4729

# Dynamic Analysis With Stress Mode Animation by the Integrated Force Method

Surya N. Patnaik, Rula M. Coroneos, and Dale A. Hopkins  
*Lewis Research Center*  
*Cleveland, Ohio*



National Aeronautics and  
Space Administration

**Office of Management**  
Scientific and Technical  
Information Program

**1997**

# DYNAMIC ANALYSIS WITH STRESS MODE ANIMATION BY THE INTEGRATED FORCE METHOD

Surya N. Patnaik  
Ohio Aerospace Institute  
Brook Park, Ohio 44142

Rula M. Coroneos and Dale A. Hopkins  
National Aeronautics and Space Administration  
Lewis Research Center  
Cleveland, Ohio 44135

## Summary

Dynamic animation of stresses and displacements, which complement each other, can be a useful tool in the analysis and design of structural components. At the present time only displacement-mode animation is available through the popular stiffness formulation. This paper attempts to complete this valuable visualization tool by augmenting the existing art with stress mode animation. The reformulated method of forces, which in the literature is known as the integrated force method (IFM), became the analyzer of choice for the development of stress mode animation because stresses are the primary unknowns of its dynamic analysis. Animation of stresses and displacements, which have been developed successfully through the IFM analyzers, is illustrated in several examples along with a brief introduction to IFM dynamic analysis. The usefulness of animation in design optimization is illustrated considering the spacer structure component of the International Space Station as an example. An overview of the integrated force method analysis code (IFM/ANALYZERS) is provided in the appendix.

## Introduction

Animation of displacement modes, which provides an overall visualization of the deformations, is an elegant tool for the examination of the dynamic behavior of a structure. The field of animation, however, can be improved by an augmentation in the existing art with stress mode animation. Stress and displacement animations, which complement each other, can together provide a comprehensive visual behavior of a structure. Consider, for example, a cantilevered beam. Its displacement animation depicts the motion of the beam with the maximum amplitude occurring at its free end. Fundamental stress-mode animation, on the other hand, shows peak stress response at its built-in end where displacements are suppressed. Both stress and displacement animations can be useful for design, fatigue, and fracture studies of the beam.

Displacement animation can be obtained by coupling the popular MSC/NASTRAN stiffness code (ref. 1) with the "Insight" animation feature of the Patran software (ref. 2). Several other commercial codes (ASKA, ANSYS, ABACUS, etc.) (refs. 3 to 5) can also be used for displacement animation. Displacement formulation, as the basis of these codes, can pose difficulty for stress field animation because stresses are not the primary unknowns of its dynamic eigenvalue analysis. Furthermore, stress prediction by the stiffness method can be liable to accuracy deficiency, and as it turns out, dynamic animation of stresses has yet to be attempted through the displacement formulation. At this juncture, the reformulated method of forces, which in the literature is known as the integrated force method (IFM) (refs. 6 to 8), becomes a valuable alternate tool for animation of the stress fields especially because stresses are the primary unknowns of its dynamic analysis. The IFM, which produces accurate stresses and displacements (refs. 6 and 7), has been extended to include the dynamic animation of both stress and displacement fields. Additionally, animation has been used in design optimization to generate simpler structures which can facilitate fabrication.

This paper, which discusses stress and displacement animations and their use in design optimization, is divided into five subsequent sections. Section 2 includes the IFM equations, dual formulation, an illustrative example, and animation procedure. Numerical examples are presented in section 3. Section 4 provides a brief summary of the use of animation in design optimization, followed by conclusions in section 5. An overview of the IFM/ANALYZERS is given in the appendix.

## Equations of the Integrated Force Method

In the integrated force method (IFM), a discretized structure for analysis, is designated by two attributes  $n$  and  $m$ . The number of unknown forces or force degrees of freedom ( $fof$ ) is  $n$ . Likewise, the displacement degrees of freedom ( $dof$ ) is  $m$ . If  $fof = dof$ , then the structure is determinate ( $r = n - m = 0$ ) and its analysis is trivial. For indeterminate structures,  $fof$  exceeds

$dof$  and the degree of indeterminacy of the structure is  $r = dof - dof = n - m > 0$ . The governing IFM equations are obtained by coupling  $m$  equilibrium equations and  $r$  compatibility conditions. The equations of the integrated force method are summarized next (refs. 6 and 7).

Static analysis equations of the IFM are as follows:

$$\begin{bmatrix} [B] \\ [C][G] \end{bmatrix} \bar{F} = \begin{bmatrix} \bar{P} \\ \bar{\delta R} \end{bmatrix} \quad (1a)$$

or

$$[S] \bar{F} = \bar{P}^* \quad (1b)$$

where  $[B]$  is the  $(m \times n)$  equilibrium matrix,  $[C]$  is the  $(r \times n)$  compatibility matrix,  $[G]$  is the concatenated symmetrical flexibility matrix of dimension  $(n \times n)$ ,  $\bar{P}$  is the  $m$  component load vector,  $\bar{\delta R}$  is the  $r$  component effective initial deformation vector, and in the absence of initial deformations it is a null vector  $\{\bar{\delta R}\} = \{0\}$ , and  $[S]$  is the  $(n \times n)$  governing the IFM matrix. The matrices  $[B]$ ,  $[C]$ ,  $[G]$ , and  $[S]$  are banded and have full row ranks of  $m$ ,  $r$ ,  $n$ , and  $n$ , respectively. The solution of equation (1) yields the  $n$  forces  $\bar{F}$ . Forces, in other words, can be determined without any reference to displacements provided the structure is kinematically stable. The  $m$  displacements  $\bar{X}$ , if required, can be obtained from forces by backsubstitution as:

$$\bar{X} = [J][G] \bar{F} \quad (2)$$

Here,  $[J]$  is the  $m \times n$  deformation coefficient matrix defined as:

$$[J] = m \text{ rows of } [S]^{-1} \quad (3)$$

The frequency analysis equation of the IFM without damping is as follows:

$$\left[ [S] - \omega^2 \begin{bmatrix} [M][J][G] \\ 0 \end{bmatrix} \right] \bar{F} = 0 \quad (4)$$

where  $[M]$  is the  $(m \times m)$  mass matrix,  $\omega$  is the circular frequency, and  $\bar{F}$  is the force mode shape of the eigenvalue problem.

Forces are the unknowns of the IFM vibration analysis. Displacement modes in IFM, if required, can be backcalculated from forces  $\bar{F}$  using equation (2). In other words, the IFM provides one set of equations to determine forces (eq. (1) for static or eq. (2) for vibration analysis), and another set for the calculation of displacements (eq. (2)).

The dual integrated force method (IFMD) is obtained by mapping forces into displacements (ref. 7). The basic equations of the dual formulation neglecting initial deformations and damping are summarized next.

Static analysis equations of the IFMD are as follows:

$$[D] \bar{X} = \bar{P} \quad (5)$$

Forces can be obtained from displacements using the following formulae:

$$\bar{F} = [G]^{-1} [B]^T \bar{X} \quad (6)$$

Dynamic analysis equations of the IFMD are as follows:

$$[D] - \omega^2 [M] \bar{X} = 0 \quad (7)$$

where the  $(m \times m)$  symmetrical matrix  $[D] = [B][G]^{-1}[B]^T$ , is assembled at element level.

From the displacement modes, force mode shapes can be backcalculated using equation (6). Like IFM, the dual IFMD, which treats displacements as the primary variables, has one equation to calculate displacements (eq. (5) for static or eq. (7) for dynamic analysis), and one equation for the determination of forces from displacements (eq. (6)). Both IFM and IFMD provide identical solution for stresses, displacements, and frequencies. For design and sensitivity analysis, the primal IFM, however, has some advantage over the dual IFMD (refs. 9 and 10).

The IFM for dynamic analysis was introduced for simple examples well over a decade ago (ref. 8). Since then, several improvements have been incorporated into the reformulated method of forces such as the generation of compatibility conditions (ref. 11), development of the dual formulation (ref. 7), and design sensitivity calculations (ref. 9), just to mention a few. To familiarize the reader with the IFM/IFMD solution process, the example of a cantilevered beam is discussed in brief. The beam is 12 in. long, 2 in. deep, and 1/4 in. thick. It is made of steel with Young's modulus  $E = 30\,000$  ksi, Poisson's ratio  $\nu = 0.3$ . The beam, which is considered massless for dynamic analysis, has two lumped masses of weight 5 lb each, as shown in figure 1. For the purpose of illustration, the beam is discretized by two QD04\_05 membrane elements of IFM/ANALYZERS (see the appendix) as shown in figure 1. The QD04\_05 is a four-node quadrilateral element and its  $dof = 8$  and  $fof = 5$ . The beam discretized by the two elements has  $dof = 8$  and  $fof = 10$  and it is a two-degree indeterminate structure.

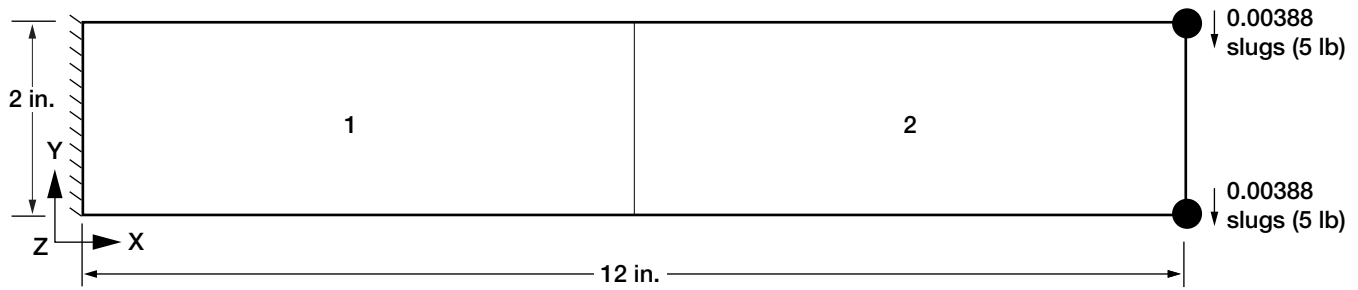


Figure 1.—Cantilevered beam idealized by two QD04\_05 membrane elements of IFM/ANALYZERS.

The frequency equations for the beam, explicitly written for IFM, IFMD, and the stiffness method, are presented next. In the IFM/ANALYZERS code, which is introduced in the appendix, the stiffness method has been included for the purpose of comparison of numerical results.

The IFM frequency equation

$$\left[ [S] - \omega^2 \begin{bmatrix} [M] & [J] & [G] \\ 0 & & \end{bmatrix} \right] \bar{F} = 0$$

for the cantilevered beam depicted in figure 1 has explicit form of equation (8).

$$\left[ \begin{array}{cccccccccc} 1 & 0 & -3 & -1/3 & 0 & -1 & 0 & -3 & 1/3 & 0 \\ 0 & -3 & 1 & 0 & -3 & 0 & -3 & -1 & 0 & 3 \\ 0 & 0 & 0 & 0 & 0 & 1 & 0 & -3 & -1/3 & 0 \\ 0 & 0 & 0 & 0 & 0 & 0 & -3 & 1 & 0 & -3 \\ 0 & 0 & 0 & 0 & 0 & 1 & 0 & 3 & 1/3 & 0 \\ 0 & 0 & 0 & 0 & 0 & 0 & 3 & 1 & 0 & 3 \\ 1 & 0 & 3 & 1/3 & 0 & -1 & 0 & 3 & -1/3 & 0 \\ 0 & 3 & 1 & 0 & 3 & 0 & 3 & -1 & 0 & -3 \\ - & - & - & - & - & - & - & - & - & - \\ 5^* & -2^* & 0 & 0 & 5^* & 0 & 0 & 0 & 0 & 0 \\ -10^* & 3^* & 0 & 0 & 0 & 5^* & -2^* & 0 & 0 & 5^* \end{array} \right] - \omega^2 \times 10^{-8} \left[ \begin{array}{cccccccccc} 0 & 0 & 0 & 0 & 0 & 0 & 0 & 0 & 0 & 0 \\ 0 & 0 & 0 & 0 & 0 & 0 & 0 & 0 & 0 & 0 \\ 0.3 & -0.06 & 0 & -0.3 & -0.06 & 0.3 & -0.09 & 0 & -0.31 & 0.02 \\ -\epsilon^a & 0.02 & 0.8 & -2.8 & 0.02 & 0.02 & -0.07 & 0.8 & -0.93 & -0.11 \\ 0.3 & -0.06 & 0 & 0.3 & -0.06 & 0.3 & -0.09 & 0 & 0.31 & 0.02 \\ \epsilon^a & -0.02 & 0.8 & -2.8 & -0.02 & -0.02 & 0.07 & 0.8 & -0.93 & 0.11 \\ 0 & 0 & 0 & 0 & 0 & 0 & 0 & 0 & 0 & 0 \\ 0 & 0 & 0 & 0 & 0 & 0 & 0 & 0 & 0 & 0 \\ 0 & 0 & 0 & 0 & 0 & 0 & 0 & 0 & 0 & 0 \\ 0 & 0 & 0 & 0 & 0 & 0 & 0 & 0 & 0 & 0 \end{array} \right] \bar{F} = 0 \quad (8)$$

The last two rows in the [S] matrix are small numbers which in equation (8) are rounded up, for example,  $5^* = 4.8 \times 10^{-7}$  and  $2^* = -1.6 \times 10^{-6}$ , etc. Also,  $\epsilon^a = 0.0066$ .

The IFM eigenvalue problem for the beam is an unsymmetrical (10 × 10) set of equations. The first eight equations (see eq. (8)) represent the equilibrium conditions, whereas the last two equations are the compatibility conditions. The four

nonzero rows in the mass matrix represent the participation of lumped masses which are located at nodes 3 and 4. Participation of all 10 dof is essential for the determination of correct frequency and force mode shapes (refs. 7, 8, and 10). A correct dynamic analysis formulation cannot be obtained through any elaborate manipulation of the equations of the classical force method (ref. 12), because this approach does not consider the mass or the inertia for redundant members. The four frequen-

cies obtained for the problem are given in table I. The fundamental force mode shape along with the displacement mode shape calculated by backsubstitution using equation (2) are shown in table II.

The IFMD frequency equation  $\left[ [D] - \omega^2 [M] \right] \bar{X} = 0$  for the two-element cantilevered beam depicted in figure 1 has the explicit form of equation (9).

TABLE I.—FREQUENCIES FOR A CANTILEVERED BEAM WITH LUMPED MASS

Frequency numbers	Frequencies in Hz			
	IFM	IFMD	Stiffness method	Analytical solution
	Frequency, Hz			
1	170.629	170.629	353.073	168.32
2	2031.261	2031.261	2032.188	1052.00
3	2534.278	2534.278	4874.846	2950.38
4	9298.475	9298.475	9599.293	5786.00

TABLE II.—FORCE AND DISPLACEMENT MODE SHAPES FOR FUNDAMENTAL FREQUENCY OF CANTILEVERED BEAM

IFM		IFMD		Stiffness method <sup>a</sup>
Force mode shape	Displacement mode shape	Force mode shape	Displacement mode shape	Displacement mode shape
0.0	$9.78 \times 10^{-2}$	0.0	$9.78 \times 10^{-2}$	$9.17 \times 10^{-2}$
0.0	0.303	0.0	0.303	0.315
$-3.65 \times 10^{-2}$	0.131	$-3.65 \times 10^{-2}$	0.131	0.123
1.0	1.0	1.0	1.0	1.0
0.0	-0.131	0.0	-0.131	-0.123
0.0	1.0	0.0	1.0	1.0
0.0	$-9.78 \times 10^{-2}$	0.0	$-9.78 \times 10^{-2}$	$-9.18 \times 10^{-2}$
$-3.65 \times 10^{-2}$	0.303	$-3.65 \times 10^{-2}$	0.303	0.315
0.343	-----	0.343	-----	-----
0.0	-----	0.0	-----	-----

<sup>a</sup>Force mode shape cannot be determined.

$$\begin{bmatrix}
 10^6 & \begin{bmatrix}
 6.1 & 0.0 & 1.3 & -0.1 & -2.6 & -1.3 & -3.44 & 0.0 \\
 & 16.6 & 0.1 & 4.0 & -1.3 & -4.5 & 0.0 & -15.6 \\
 & & 3.0 & -1.3 & -1.7 & -0.1 & -2.6 & 1.34 \\
 & & & 8.3 & 0.1 & -7.8 & 1.3 & -4.5 \\
 & & & & 3.0 & 1.3 & 1.3 & -0.1 \\
 & & & & & 8.3 & 0.1 & 4.0 \\
 & & & & & & 6.1 & 0.0 \\
 & & & & & & & 16.6
 \end{bmatrix} & -\omega^2 \times 10^{-3} & \begin{bmatrix}
 0 & & & & & & & & \\
 & 0 & & & & & & & \\
 & & 4 & & & & & & \\
 & & & 4 & & & & & \\
 & & & & 4 & & & & \\
 & & & & & 4 & & & \\
 & & & & & & 0 & & \\
 & & & & & & & 0 & \\
 & & & & & & & & 0
 \end{bmatrix}
 \end{bmatrix} \vec{X} = 0 \quad (9)$$

There are eight equations for the dual method. The four nonzero entries in the diagonal mass matrix in equation (9) correspond to the lumped masses. The structure of the IFMD eigenvalue equation appears similar to standard stiffness equations. The differences between IFMD and the stiffness equations is examined later in this paper. The frequencies obtained by IFMD are given in table I. The fundamental displacement mode shape

along with the force mode, backcalculated using equation 6, are shown in table II. Notice that the frequencies obtained as solutions to IFM equation (4) and IFMD equation (7) agreed with each other. Both force and displacement mode shapes given in table II also agreed for IFM and IFMD. Henceforth, no distinction will be made for results generated either by IFM or IFMD.

The IFM equations are unsymmetrical while those for dual are symmetrical. Either set of equations can be used to obtain frequency, stress, and displacement mode shapes. The symmetrical form can use popular eigenvalue solution routines (such as DSPGV) which is readily available in the LAPACK public domain library (ref. 13). For unsymmetrical eigenvalue analysis, LAPACK routine DGEQV is used (ref. 13). For static analysis, the Harwell library routines (MA28AD, MA28CD, MA29BD, MA29CD, MA47AD, MA47BD, MA47CD, MA47ID) are used (ref. 14). However, it is observed that the unsymmetrical IFM version can be more useful than IFMD in design and sensitivity analysis (ref. 10). Furthermore, the IFM solution which provides  $r = n - m$  number of zero frequencies and associated eigenvectors corresponding to the  $r$  number of compatibility conditions can be used to verify solution accuracy.

For the purpose of comparison, the stiffness analysis is also provided for the beam. The element used for the stiffness analysis has four nodes and eight displacement degrees of freedom. The stiffness element uses displacement fields identical to the IFM/IFMD element QD04\_05. In IFM/ANALYZERS (see the appendix) this stiffness element is also referred to as QD04\_05. The IFM/ANALYZERS, in other words, retains the same element name for different analysis methods such as the IFM, IFMD, and stiffness methods. The analysis method is specified through a set of executive control keywords, which can be IFM!, IFMD!, or STIFF!, for primal, dual, or stiffness analysis, respectively. Generation of all elemental matrices of the IFM, IFMD, and stiffness methods use identical numerical integration and are programmed in the Fortran 77 language. For the problems, the IFM, IFMD, and stiffness elements used are considered equivalent. All numerical results have been obtained on the Cray-YMP 8E/8128 supercomputer at the NASA Lewis Research Center.

The stiffness method frequency equations  $[[K] - \omega^2 [M]] \bar{X} = 0$  for the cantilever beam depicted in figure 1 have the explicit form of equation (10). Frequency and displacement modes obtained are presented in tables I and II. Calculation of stress mode shapes is not readily available in the stiffness method.

## Comparison of IFM, IFMD, and Stiffness Results

From the solution of the cantilevered beam, the following observations can be made for the IFM, IFMD, and stiffness methods.

Both the primal IFM and the dual IFMD provide identical solutions for frequencies, stress, and displacement mode shapes (see tables I and III).

Results for the integrated force method are more accurate than those for the stiffness method. For IFM, the two-element model of the beam produced accurate fundamental frequency with an error of about one percent. The error in the fundamental frequency for the stiffness method, however, is about 110 percent. The higher modal frequencies given in table I are in error because of the crude two-element model and are not further discussed. Force and displacement mode shapes obtained by IFM and IFMD agreed as expected (see table II). The stiffness method displacement mode exhibits some error even for this modest example (see table II).

The cause of higher fundamental frequency in the stiffness method can be observed from a comparison of equation (9) for IFMD and equation (10) for the stiffness method. Mass matrices for both stiffness and IFMD (eqs. (9) and (10)) are identical. The coefficient of the  $[K]$  matrix in stiffness equation (10) differs from that of the  $[D]$  matrix in IFMD equation (9). For this problem, all eight diagonal elements in matrix  $[K]$  are bigger than the corresponding entries in the matrix  $[D]$ . In other words, a higher frequency for the stiffness method was anticipated because the stiffness equation (eq. (10)) is stiffer than the IFMD equation (eq. (9)).

$$\begin{bmatrix} 10^6 & \begin{bmatrix} 7.6 & 0.0 & 0.5 & -0.1 & -1.9 & -1.3 & -4.8 & 0.0 \\ & 17.1 & 0.1 & 4.8 & -1.4 & -4.3 & 0.0 & -16.1 \\ & & 3.8 & -1.3 & -2.4 & -0.1 & -1.9 & 1.3 \\ & & & 8.6 & 0.1 & -8.1 & 1.3 & -4.3 \\ & & & & 3.8 & 1.3 & 0.5 & -0.1 \\ & & & & & 8.6 & 0.1 & 3.8 \\ & & & & & & 7.6 & 0.0 \\ & & & & & & & 17.1 \end{bmatrix} \\ & \text{sym} \end{bmatrix} - \omega^2 \times 10^{-3} \begin{bmatrix} 0 & & & & & & & \\ & 0 & & & & & & \\ & & 4 & & & & & \\ & & & 4 & & & & \\ & & & & 4 & & & \\ & & & & & 4 & & \\ & & & & & & 4 & \\ & & & & & & & 0 \\ & & & & & & & & 0 \end{bmatrix} \bar{X} = 0 \quad (10)$$



TABLE III.—RESULTS FOR AN ISOTROPIC  
CANTILEVERED BEAM

Model	IFM/IFMD	Stiffness method	MSC/NASTRAN <sup>a</sup>
	Frequency, <sup>b</sup> Hz (1,3)		
CB_Model_1	1.005	1.637	1.637
Six/HX08_18	1.043	1.640	1.640
CB_Model_2	1.007	1.014	1.014
Six/HX20_90	0.983	0.995	0.995
CB_Model_3	1.021	2.672	2.672
Three/HX08_18	1.274	1.862	1.862
CB_Model_4	1.025	1.041	1.041
Three/HX20_90	1.069	1.091	1.091
CB_Model_5	1.014	2.335	2.335
Three/HX08_18 (irregular mesh)	1.516	1.887	1.887

<sup>a</sup>Equivalent MSC/NASTRAN elements (CHEXA with 8 nodes or CHEXA with 20 nodes) are used.

<sup>b</sup>Frequencies are normalized with respect to strength of material formulae.

## Dynamic Animation of Stress Mode Shape

Stress is a second-order tensor with six components at every point of a solid continuum. Thus, the solid modeler solution of the IFM/ANALYZERS has six stress components at each node. Animations of a second-order tensor quantity is a cumbersome proposition, and it can also be difficult to visualize. Fortunately, however, failure in a structure can be attributed to a single quantity such as von-Mises stress, which is a scalar function of the six stress components and can be written as:

$$\sigma_{von-M} = \sqrt{\frac{1}{2} \left[ (\sigma_x - \sigma_y)^2 + (\sigma_y - \sigma_z)^2 + (\sigma_z - \sigma_x)^2 \right] + 3(\tau_{yz}^2 + \tau_{zx}^2 + \tau_{xy}^2)} \quad (11)$$

Stress animation, in other words, represents animations of the von-Mises stress given by equation (11). Von-Mises stress animation is consistent with the animation of the scalar displacement magnitude in the stiffness method that is available at the present time. Equivalent von-Mises stress is calculated for the force eigenvector obtained from the solution of IFM dynamic equation (4) or equation (7) for IFMD. Dynamic animation for stress and displacement modes is obtained by supplementing the “Insight” tool of the P3/Patran software with force mode solutions through Patran neutral files. For example, the animation of stress modes requires the preparation of two neutral files. The first file should include the finite element data, which contains the nodal coordinates and element connectivities in the model. The second file should contain the von-Mises stress for each node and the frequency.

The determination of von-Mises stress for three-dimensional solid elements (of IFM/ANALYZERS), which are represented by complete polynomials, can be quite tedious but it is easy to calculate in a computer. The IFM/ANALYZERS provides both displacement and stresses (including von-Mises stresses) at the grid points and other specified locations. For completeness, von-Mises stress calculation is illustrated for a simple rectangular membrane element QD04\_05 used in example 1. The three stress components for this membrane element can be obtained as:

$$\sigma_x = \frac{F_1}{t} + \frac{F_2}{t} (2y/a)$$

$$\sigma_y = \frac{F_3}{t} + \frac{F_4}{t} (2x/b) \quad (12)$$

$$\tau_{xy} = \frac{F_5}{t}$$

where  $(\sigma_x, \sigma_y, \tau_{xy})$  are membrane stresses,  $(F_1, F_2, \dots, F_5)$  are force mode shapes for element QD04\_05,  $t$  is the element thickness, and  $a$  and  $b$  are the dimension of the QD04\_05 element along the  $x$  and  $y$  coordinates, respectively. For the membrane element, the von-Mises stress given in equation (11) can be calculated by substituting  $(\sigma_x, \sigma_y, \text{ and } \tau_{xy})$  from equation (12) and setting  $(\sigma_z = \tau_{zx} = \tau_{zy} = 0)$ .

Two features of P3/Patran fringe plotting and modal animating, which control time and space, are used to display the animation results. Animations can be viewed best by using an audio-video VCR system. A videotape, which contains the stress and displacement animation for several examples (ref. 15), is available and can be sent on request. In this paper, however, only a single-frame animation depicting maximum response can be presented. A single animation frame is obtained by pausing the setup to approximately correspond to peak response regime and then taking a “snap-shot”, which is available in the Silicon Graphics Indy Unix workstation used for the purpose. Displacement animation is obtained by replacing stress results in favor of displacement mode shapes.



## Numerical Examples

Results for three examples, a cantilevered beam (example 2), an L\_Beam (example 3), and a turboprop blade (example 4) obtained with IFM/ANALYZERS, are summarized next. The material used for all the examples is steel with properties identical to that of example 1 with mass density  $\rho = 0.289$  lb/cu in. The frequency results were obtained for distributed self-mass of the structure using a consistent mass matrix formulation. The structures were discretized using an eight-node solid element HX08\_18 and a twenty-node solid element HX20\_90. The structures with principal dimensions are depicted in figure 2. Again, solutions are obtained by using IFM, IFMD, and the stiffness method. Results obtained by the MSC/NASTRAN analyzer using comparable elements are also given. For each example, a single frame from the dynamic animation depicting the peak stress and displacement modes is included.

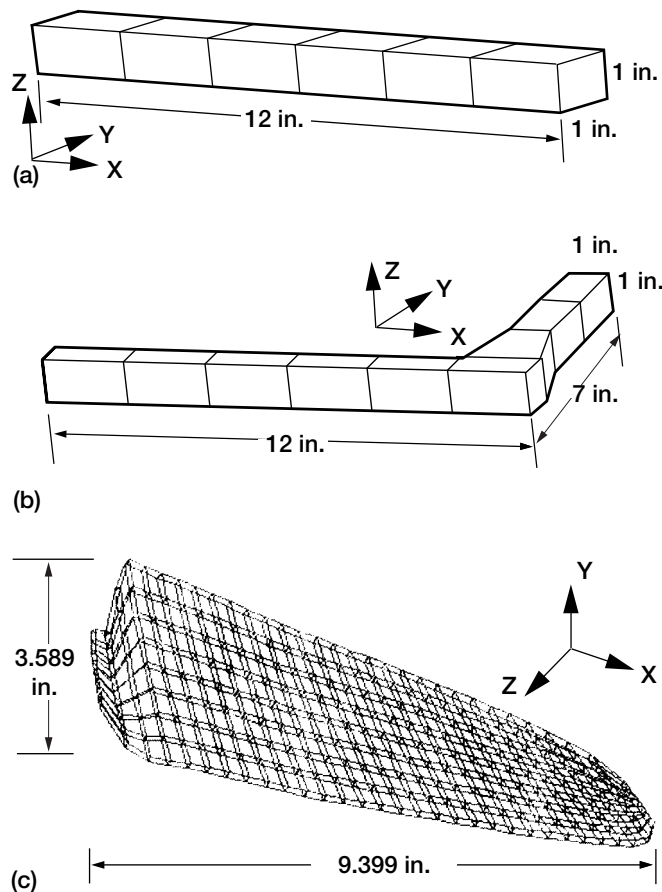


Figure 2.—Overall geometrical dimensions of examples.  
 (a) Example 2: Cantilevered beam idealized by six solid elements.  
 (b) Example 3: Cantilevered L\_beam idealized by nine solid elements.  
 (c) Example 4: Turboprop blade idealized by 240 solid elements.

### Example 2: Cantilevered Beam

Results for the cantilevered beam, shown in figure 3, obtained using IFM, IFMD, and the stiffness method, are depicted in table III. Five finite element models are used for this example. CB\_Model\_1 has six, eight-node, HX08\_18 solid elements. CB\_Model\_2 has six, twenty-node, HX20\_90 solid elements. CB\_Model\_3 is similar to CB\_Model\_1 but only three elements are used. Likewise, CB\_Model\_4 has three elements but is otherwise similar to CB\_Model\_2. CB\_Model\_5 has a total of three elements, one small element near the support and two other elements. For MSC/NASTRAN analysis, the same models are used but IFM/ANALYZERS elements HX08\_18 and HX20\_90 are replaced by equivalent elements. That is, IFM/ANALYZERS elements HX08\_18 and HX20\_90 are replaced by equivalent MSC/NASTRAN elements (CHEXA with eight nodes and CHEXA with twenty nodes, respectively). First and third frequencies for the beam, obtained by different methods, are given in table III (second frequency is identical to the fundamental mode due to symmetry). Results are normalized with respect to the strength of material beam solutions. The beam solutions are quite accurate; however, there can be some difference in the results due to three-dimensional elasticity and boundary restraint effects. For example, a beam model uses one material constant, which is Young's modulus, whereas a three-dimensional elasticity solution uses Poisson's ratios in addition.

For this problem, IFM/IFMD results for the fundamental frequency are found to be quite accurate. The six-element models CB\_Model\_1 and CB\_Model\_2 have a margin of error of 0.5 percent and 0.7 percent, respectively. The crude three-element models CB\_Model\_3 and CB\_Model\_4 exhibit somewhat higher margins of error. More error is noticed for the third mode, as anticipated, because the finite element discretization represents a coarse mesh. Results obtained by using the stiffness method and MSC/NASTRAN software agreed since both are based on displacement formulation. For the fundamental frequency, a higher order MSC/NASTRAN element (CHEXA with twenty nodes) which is equivalent to IFM/ANALYZERS element HX20\_90 produced acceptable results (see results for CB\_Model\_2 and CB\_Model\_4 in table III). The solution obtained by the normal eight-node element of the stiffness method and the eight-node CHEXA MSC/NASTRAN element provide a poor comparison with the eight-node IFM/ANALYZERS HX08\_18 element.

For this example, von-Mises stress and displacement animation have been obtained by using IFM/ANALYZERS and Patran software. A single-frame animation picture for fundamental displacement and stress modes is depicted in figure 4 for CB\_Model\_2. In figure 4, the neutral axis of the beam is clearly visible and maximum von-Mises stress occurs near the support. Von-Mises stress is symmetrical with respect to the neutral plane, which at times can be color-camouflaged.

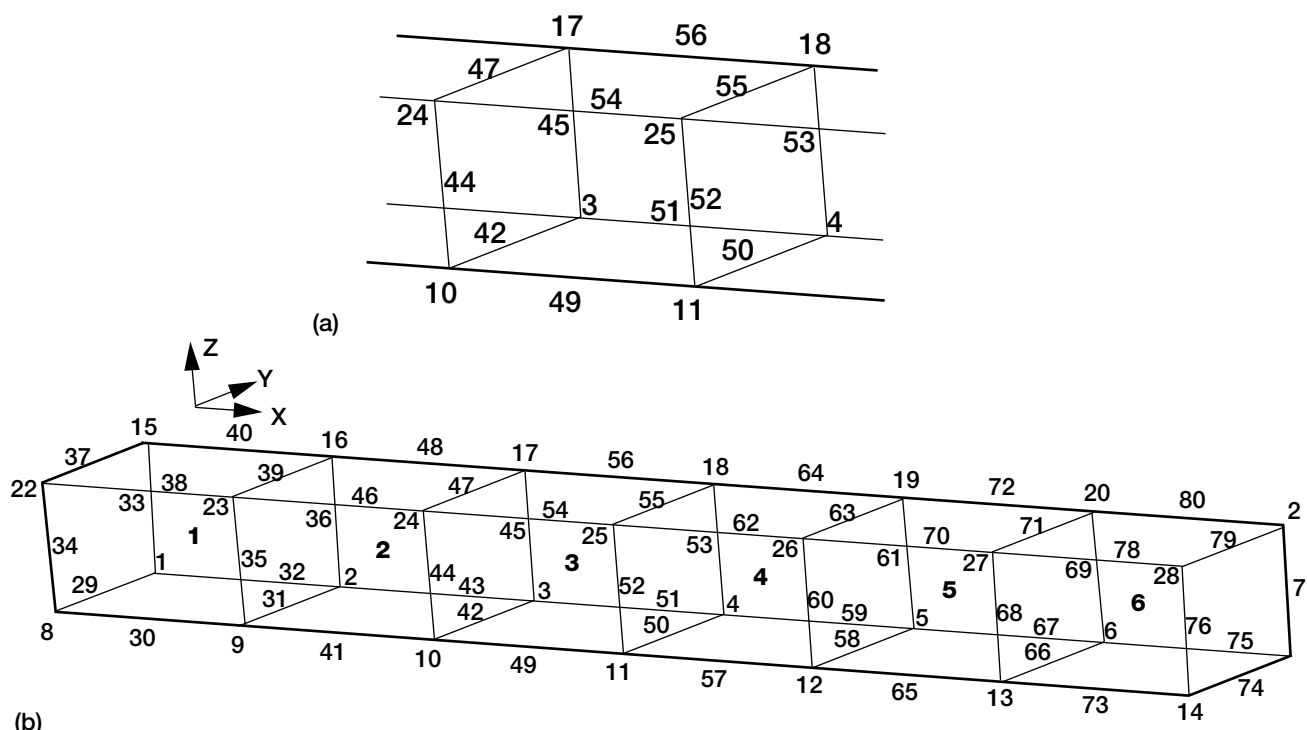


Figure 3.—Cantilevered beam idealized by six HX20\_90 solid elements. (a) Enlarged view of the twenty-node element. (b) Full beam view.

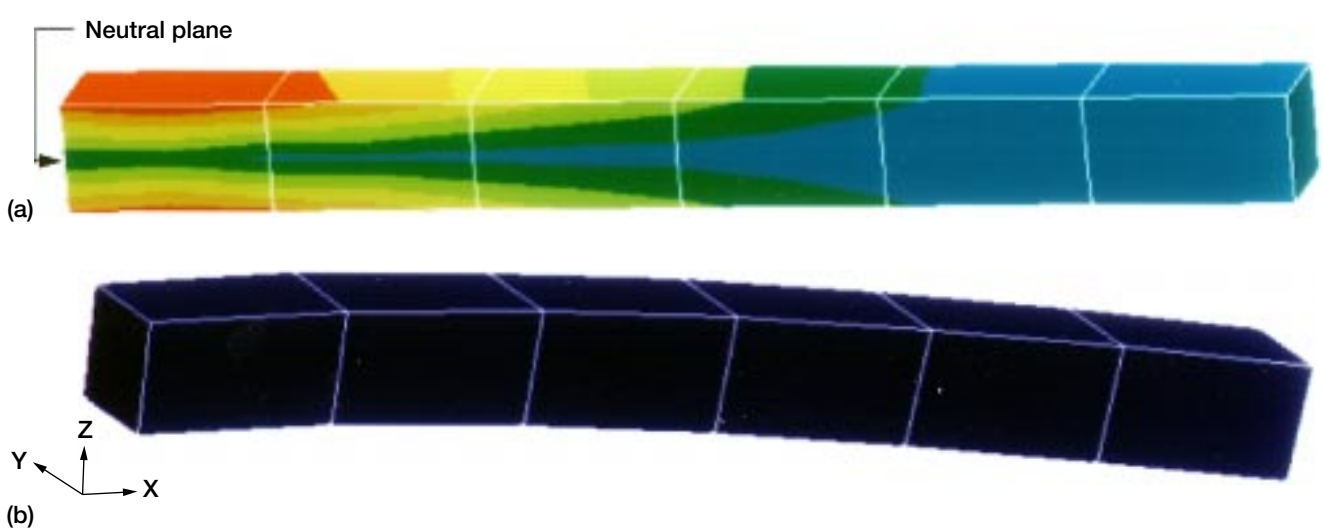


Figure 4.—First mode animation of cantilevered beam. (a) Stress mode. (b) Displacement mode.

The displacement animation frame shows maximum displacement at the free end of the cantilever. The displacement animation using the stiffness method or MSC/NASTRAN code, are found to be similar to IFM/ANALYZERS results. As stated earlier, stress field animation can not be obtained by the displacement method.

### Example 3: L\_Beam

Analysis of an L\_beam, shown in figure 2(b) is carried out by four different methods (IFM, IFMD, stiffness, and MSC/NASTRAN) for four finite element models. LB\_Model\_1 has nine, eight-node HX08\_18 solid elements; LB\_Model\_2 has nine, twenty-node HX20\_90 solid elements; LB\_Model\_3 is similar to LB\_Model\_1 except only five elements are used, and LB\_Model\_4, likewise, has five elements but is otherwise similar to LB\_Model\_2. The finite element model 2 for the L\_beam is shown in figure 5. First and third frequencies obtained by IFM/IFMD, the stiffness method, and MSC/NASTRAN are presented in table IV. Results are normalized with respect to the IFM/IFMD solution for LB\_Model\_2. For this problem it is observed that the IFM/IFMD results for the fundamental frequency are accurate with a maximum error of 3.8 percent for LB\_Model\_4 (with five HX20\_90 elements). IFM/IFMD results for the third mode are acceptable with somewhat higher error margins. Results for the stiffness method and MSC/NASTRAN agreed. However, frequency results obtained using the stiffness method and MSC/NASTRAN software are poorer than corresponding IFM solutions. MSC/NASTRAN and stiffness method performance is considered acceptable when higher order, twenty-node CHEXA elements are used for frequency analysis.

Stress and displacement animation using IFM/IFMD are obtained for the L\_Beam, for LB\_Model\_2 with nine HX20\_90 elements. A single animation frame, which corresponds to peak response for von-Mises stress mode and displacement mode, is shown in figure 6. The displacement mode for the first fundamental frequency of the L\_Beam represents motion in the plane defined by its two legs. This motion cannot be visualized through a frame taken along the L\_Beam plane. The motion can, however, be observed when a picture is taken perpendicular to the L\_Beam plane as depicted in figure 6(b). The displacement animations for LB\_Model\_2 generated by IFM

TABLE IV.—RESULTS FOR AN ISOTROPIC L\_BEAM

Model	IFM/IFMD	Stiffness method	MSC/NASTRAN <sup>a</sup>
LB_Model_1	0.999	1.451	1.451
Nine/HX08_18	1.009	1.165	1.165
LB_Model_2	1.000	1.006	1.006
Nine/HX20_90	1.000	1.003	1.003
LB_Model_3	1.024	1.720	1.720
Five/HX08_18	1.003	1.341	1.341
LB_Model_4	1.038	1.046	1.046
Five/HX20_90	1.016	1.020	1.020

<sup>a</sup>Equivalent MSC/NASTRAN element (CHEXA with 8 nodes or CHEXA with 20 nodes) is used.

<sup>b</sup>Frequencies are normalized with respect to IFM LB\_Model\_2.

element HX20\_90, compared well with the stiffness method results when higher order 20-node CHEXA elements were used. The von-Mises stress animation obtained for the IFM/ANALYZERS element HX20\_90 is shown in figure 6(a). The stress animation depicts a neutral plane along the width of the beam which corresponds to its in-plane motion. Maximum von-Mises stress occurs at the restrained boundary, which is shown in red. The free end is stress-free and is shown in blue. Variation of von-Mises stress along the beam, which peaks at the restrained end, and is null at its free end, can be seen in figure 6(a).

### Example 4: Turboprop Blade

The turboprop blade is considered as the final example. The blade, shown in figure 7, is discretized using eight-node solid elements HX08\_18. The blade has a total of 240 elements with  $dof = 1620$  and  $fof = 4320$ . The first eight frequencies of the blade, obtained by IFM/IFMD, the stiffness method, and MSC/NASTRAN analyzers, are given in table V. The fundamental frequency of the blade, obtained by the IFM/IFMD analyzer, is 41.532 Hz. The fundamental frequency obtained by the stiffness and MSC/NASTRAN analyzers agreed; however, both methods produced higher frequencies at 76.731 Hz. The other seven frequencies obtained by the stiffness and MSC/NASTRAN analyzers are higher than the IFM/IFMD analyzers by about 15 to 75 percent.

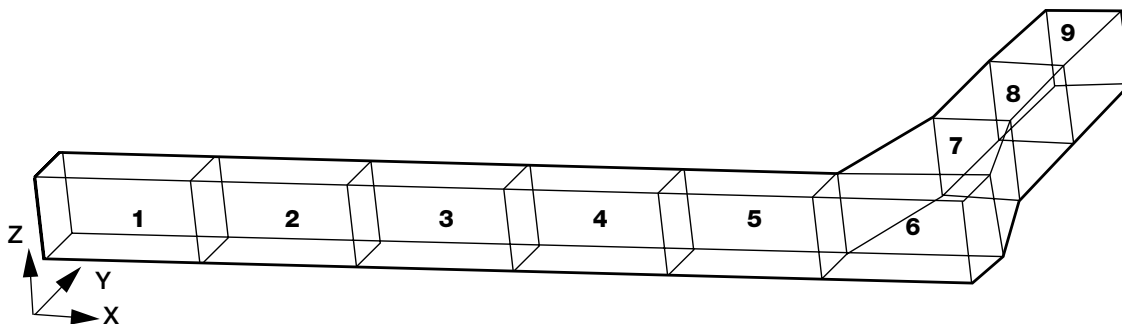


Figure 5.—L\_Beam idealized by nine solid elements.

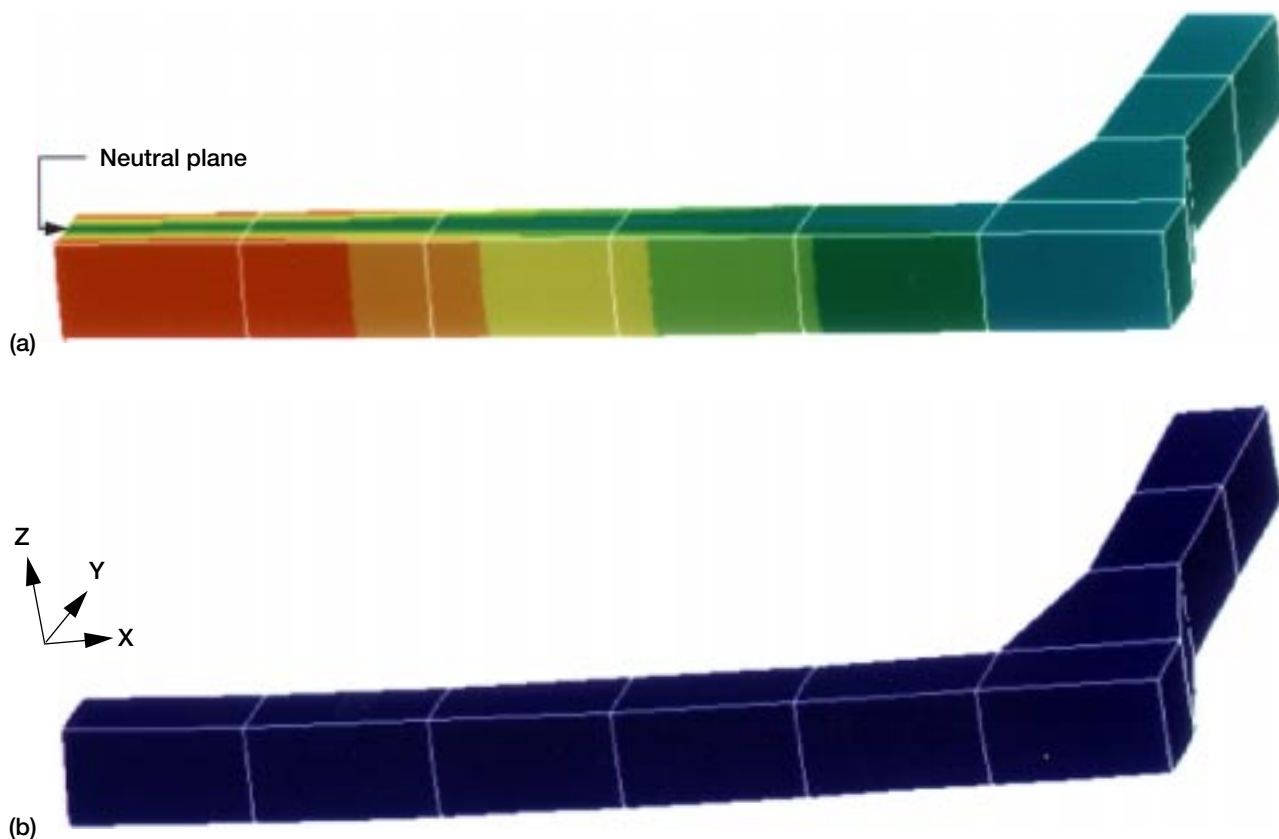


Figure 6.—First mode animation of L\_Beam. (a) Stress mode. (b) Displacement mode.

TABLE V.—FREQUENCIES FOR AN ISOTROPIC TURBOPROP BLADE IDEALIZED BY 240 (HX08\_18) SOLID ELEMENTS

Mode numbers	IFM/IFMD	Stiffness method	MSC/NASTRAN <sup>a</sup>
1	41.532	76.371 (1.839) <sup>b</sup>	76.371 (1.839)
2	217.396	386.223 (1.777)	386.223 (1.777)
3	396.692	410.118 (1.150)	410.119 (1.150)
4	541.273	785.971 (1.452)	785.971 (1.452)
5	809.480	1148.448 (1.419)	1148.448 (1.419)
6	970.508	1465.579 (1.510)	1465.579 (1.510)
7	1369.698	2094.299 (1.529)	2094.300 (1.529)
8	1596.059	2801.503 (1.755)	2801.504 (1.755)

<sup>a</sup>Equivalent MSC/NASTRAN element (CHEXA with 8 nodes) is used.

<sup>b</sup>Quantities in parenthesis are normalized with respect to IFM solution.

Animation is carried out only for IFM/ANALYZERS solutions, since the stiffness and MSC/NASTRAN results for the blade exhibited higher margins of error. A single-frame animation for stress and displacement modes for the blades is shown in figure 8. The blade response in the fundamental mode represents flexure and torsion coupled motion, as can be seen in figure 8(a). The flexure and torsion coupled response does not depict a neutral zone. The maximum displacement amplitude occurs at the free end of the blade which also exhibits considerable torsional motion (see fig. 8(b)). Von-Mises stress amplitude reduces to zero at the free end from its peak value at the built-in boundary. Stress peaks at the support of the turbo-prop blade while the free ends are stress free, as can be seen in figure 8(a).

Determination of displacement and frequencies can be carried out by the displacement method, which can also be verified by dynamic testing. Such procedures, however, do not provide a stress state in the structure. Thus, the stress animation via the method of forces becomes a viable tool to examine the dynamic behavior of the structure, especially for stress response at stress concentration regions. The stress animation tool complements the existing displacement animation, thereby, improving the existing visualization technique.



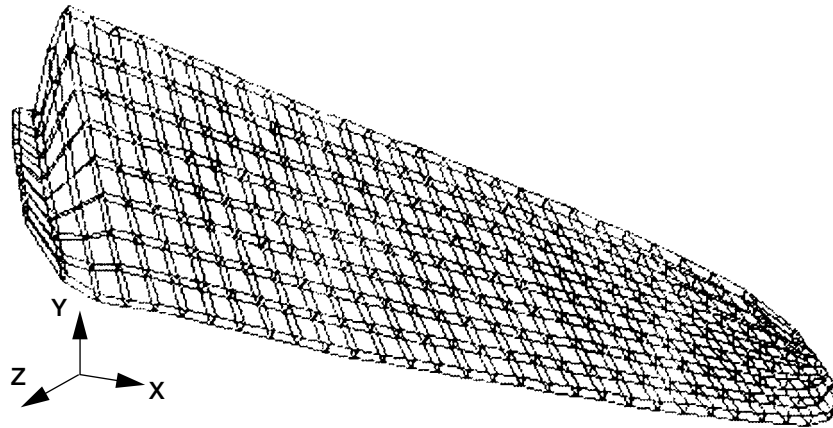
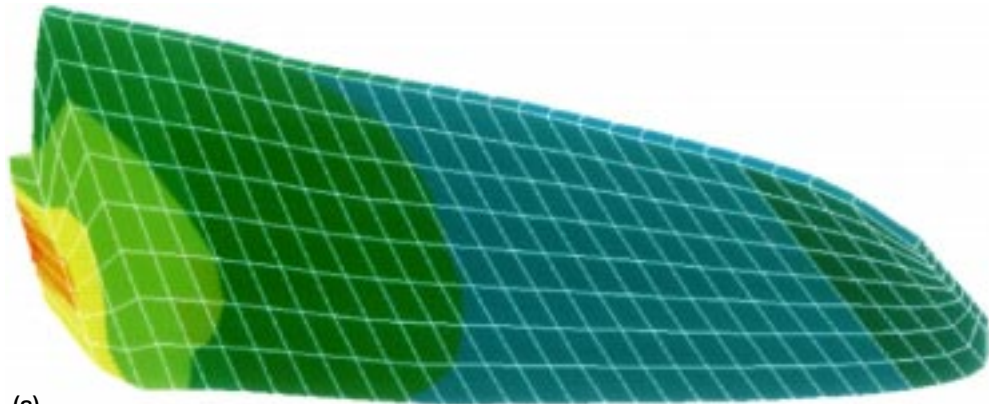
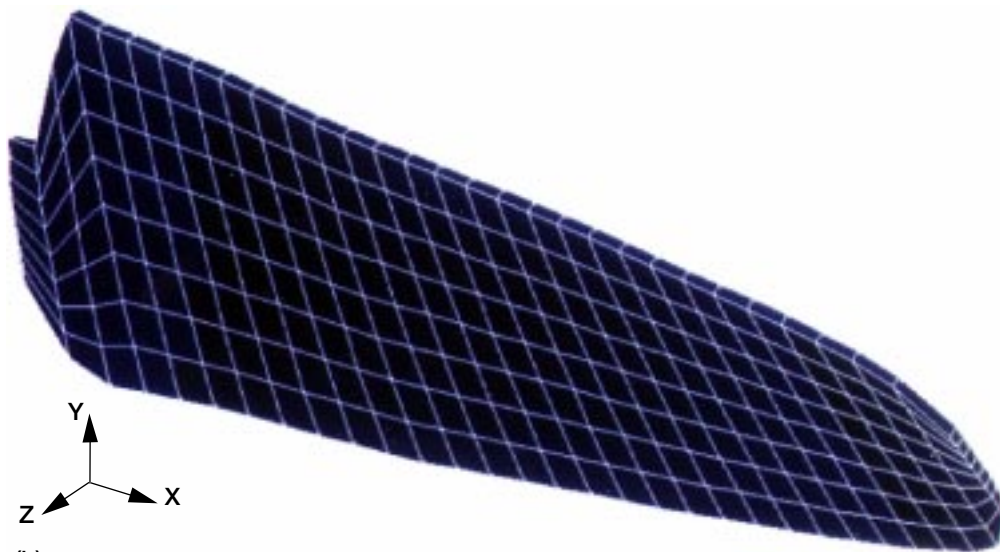


Figure 7.—Turboprop blade idealized by 240 HX08\_18 solid elements.



(a)



(b)

Figure 8.—First mode animation of turboprop blade. (a) Stress mode. (b) Displacement mode.

## Animation in Design Optimization

In the design of complex industrial structures with many variables and constraints, the optimization process can quite often be bogged down and confused, resulting in a design which cannot be easily fabricated (ref. 16). Such deficiency can be alleviated, to some extent, through cumbersome constraint manipulation schemes, which require repetition of several optimization cycles. Alleviation of the deficiency can be attempted by coupling animation to the optimization processes. Dynamic animation has been incorporated into the design tool called CometBoards (ref. 17) (which is an acronym for Comparative Evaluation Test Bed of Optimization and

Analysis Routines for the Design of Structures). The combined animation and optimization tool has been used to generate optimum designs for a number of industrial structural components. The usefulness of animation and optimization in design can be illustrated by considering the simple example of a spacer structure of the International Space Station in figure 9. The initial configuration of the spacer structure, which has 14 joints, 41 members, and weighs 500 lb, is shown in figure 9(a).

Design optimization was carried out using a finite-element model with 307 nodes and 1835 *dof* (which corresponds to 8 beam elements per frame member and 2 beam elements for the trunion (ref. 18)). This structure was designed for a number of pseudo-static and emergency-landing load conditions. The

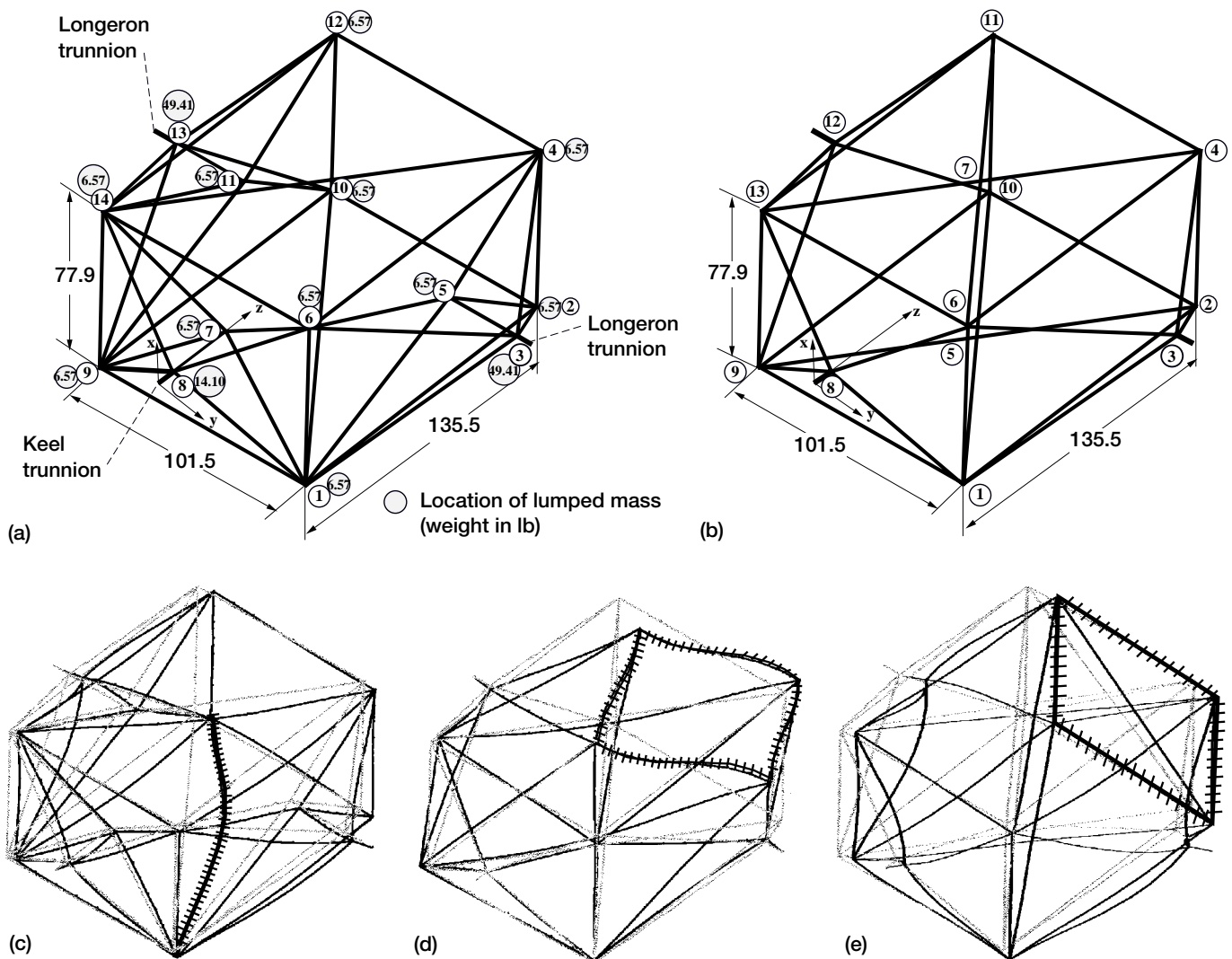


Figure 9.— Optimization and animation coupled tool produced a lighter design for the spacer structure. (a) Manual design has 14 joints, 41 members, and weight of 500 lb. (b) Optimum design has 13 joints, 32 members, and weight of 316.63 lb. (c) Dynamic animation of the manual design. Notice excessive deformation for shaded member. (d) Dynamic animation of modified configuration with open face. Notice excessive deformation for open face. (e) Dynamic animation with bracing. The deformations of the open face are reduced.

constraints considered were: stresses for all members, displacement limitations at the exterior nodes of the spacer structure for the shuttle dynamic envelope, buckling, and frequency limitations. The design was cast as a nonlinear mathematical programming problem and was solved using two optimizers (the Sequential Unconstrained Minimization Technique SUMT and the Sequential Quadratic Programming technique of the IMSL library available in CometBoards). Observations of the dynamic animation of the optimum design indicated that some members are much more flexible than others. A single animation frame for the optimum structure is shown in figure 9(c). Even from this single frame it can be seen that the member connecting nodes 1 and 10 suffer relatively large deformations compared to other members. A modified configuration, shown in figure 9(b), with fewer members (41 members of the original design were reduced to 32 members) and fewer joints (13 instead of 14 in the original configuration), was obtained through an examination of the dynamic animation of the component. The optimum design of the spacer was obtained, again, using the design tool CometBoards. The animation of the optimum design of the modified configuration indicated unacceptable excessive distortion for an open face connecting joints (2, 4, 11, 10) shown in figure 9(d). The open face is a functional on-orbit requirement for the integration of the spacer structure to the other modules of the International Space Station. This face, however, can be temporarily braced in the space shuttle during launch by a pair of turn-buckles, which weigh 2.5 lb. The bracing can be removed on orbit to allow its integration with the space station. The modified configuration, with turn-buckle bracing, was optimized again, and a single-frame animation of the braced structure is shown in figure 9(e). By comparing figure 9(d) with 9(e), it can be observed that the open face does not suffer excessive deformation. The final optimum design has a weight of 316.63 lb, which is 36 percent lighter than the manual design of 500 lb. The optimum structure has fewer members and nodes which facilitates its manufacturability. The fundamental mode of the final design is a breathing type of mode in which the entire structure participates as a single unit. In other words, the load path is well distributed amongst all members of the spacer structure. Without the use of animation, the generation of a lighter manufacturable optimum structure would have been difficult if not impossible. The animation and optimization combined tool has successfully generated an optimum manufacturable design for the spacer structure.

## Usefulness of Animation in Analysis and Design

During the qualification of industrial products through prototype testing, failures quite often occur even though modern analysis and test methods have reduced the number of such

occurrences. Review of the failure data can identify the critical region which can then be redesigned and retested. Identification of a failure-prone region, which at times can elude existing techniques, is important both from financial as well as project schedule aspects. The dynamic animation of stress modes, which has been discussed in this paper, complements the existing techniques in identifying the failure-prone regions in complex structures. Dynamic animation should be carried out for the fundamental mode as well as for higher and other local modes to identify high-stress regions. To isolate those critical failure-prone regions in a structure, only the integrated force method dynamic analysis results and a computer workstation are required.

In design optimization, the modification of the configuration of a complex structure can be improved in more ways than merely changing its sizing variables. A variety of potential configuration modifications can quickly be discovered through an examination of the dynamic animation of the structure. Scrutiny of such candidate configurations can be useful in designing an optimum structure for both configurational and sizing variables. In other words, optimization augmented with animation can be a viable design tool.

Overall, the art of animation discussed in this paper can be useful both in the analysis and in the design of complex structures.

## Concluding Remarks

Both stress and displacement animation, which complement each other, provide a comprehensive visual behavior of a structure. Thus far, only displacement animation was available through the stiffness method. The field of animation has now been improved through the development of stress mode animation using the integrated force method of structural analysis. IFM/ANALYZERS is the appropriate analysis tool for stress animation because stress modes are the primary variables of its eigenvalue analysis. Both stress and displacement animation, obtained for a number of examples, clearly depict stress and displacement responses, which peak at different locations in the structure. Augmentation of animation into the design tool CometBoards has successfully generated manufacturable optimum designs for a number of industrial structural components.

Lewis Research Center  
National Aeronautics and Space Administration  
Cleveland, Ohio, October 31, 1996



## Appendix—The Integrated Force Method Analysis Code (IFM/Analyzers)

The integrated force method of structural analysis, which parallels the completed Beltrami-Michell formulation in elasticity, has been established for both finite-element discrete analysis and analysis of elastic continua such as plates and shells (refs. 19 and 20). The internal forces (or stress parameters for continua) are considered as the primary unknowns of this method. The unknown forces are determined by solving a set of simultaneous equations which are obtained by augmenting the rectangular set of equilibrium equations with another rectangular system of equations expressed in terms of the same unknown forces. The augmenting system represents the strain compatibility conditions. Displacements, if required, can be obtained from forces by backcalculations. The variational formulation for the integrated force method has been completed. A dual to the primary IFM has also been formulated by mapping stresses into displacements. The dual integrated force method (IFMD), at the equation solution stage, considers displacements as its primary unknowns. Both IFM and IFMD have two separate equation sets; one for the determination of stress parameters and another for the calculation of displacements

(see eqs. (1) to (7)). Both IFM and IFMD provide identical solutions for all examples that have been solved thus far.

A finite-element structural analysis code which incorporates both the primal and the dual force methods, along with the regular stiffness formulation, has been developed especially for the analysis of airbreathing propulsion engine components. This structural analysis code, IFM/ANALYZERS, bestows simultaneous emphasis on stress equilibrium and strain compatibility conditions. The code has a modular organization, and it is written in Fortran 77 language for both sequential as well as parallel computational platforms. The IFM/ANALYZERS currently performs linear elastic analysis of structures for thermal and mechanical loads as well as free vibration analysis. The element library contains over a dozen different types of elements, some with mid-side nodes. Elements in this library can model a continuous number of arbitrary shapes such as airbreathing engine components. The numerical analysis segment of the code utilizes sparse unsymmetrical equation solvers of the Harwell subroutine library or, alternatively for

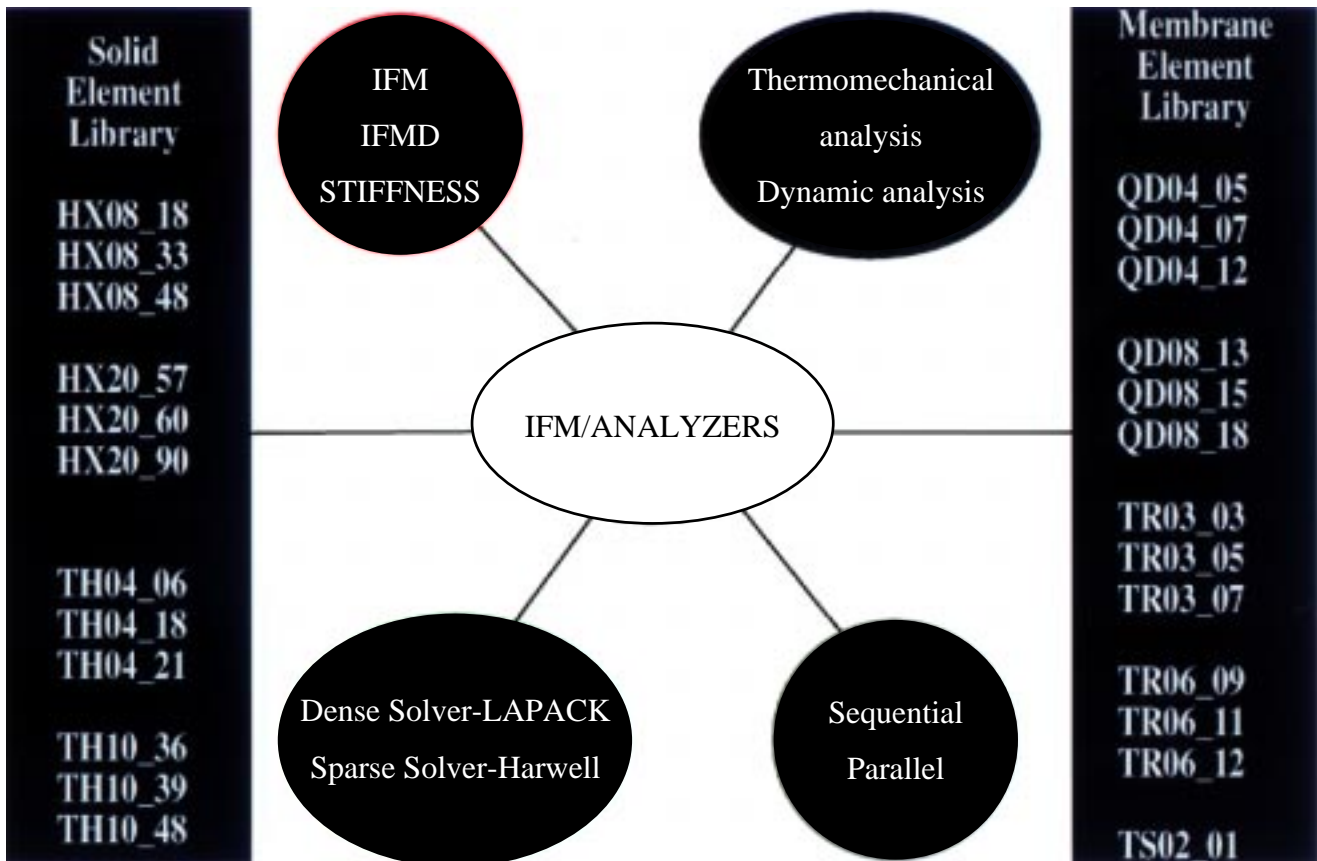


Figure 10.—Organization of IFM/ANALYZERS and its element library.

modest problems, utilizes dense solvers of the public domain LAPACK library. IFM/ANALYZERS is developed as an analysis testbed to examine the full potential of the integrated force methods since they hold promise of spawning new structural analysis tools especially for engine structure applications that can provide accurate solutions with fewer elements in the model.

Equilibrium matrix, flexibility matrix, mass matrix, thermal loads, and equivalent mechanical loads for each element are developed by discretizing potential, complementary, kinetic energies, thermal and mechanical work terms, respectively. Interpolation based on the standard stiffness method is used to

approximate displacement fields. A general formulation for stress tensor interpolation has been developed on the basis of stress function approach. The stress polynomials thus generated represent a complete set that is free from spurious zero energy modes and satisfies equilibrium in the element field. The element matrices are not sensitive to the orientation of the local coordinate systems. All elements of this library pass the “patch tests”. The organization of IFM/ANALYZERS and its element library are depicted in figure 10 and table VI. An element name (for example HX20\_90) in IFM/ANALYZERS provides the following information: The first two letters (HX) describe the geometry (HX stands for hexahedral solid element). The second two numbers (20) represent the number of nodes, here a twenty-node hexahedral element with sixty displacement degrees of freedom. The last two numbers (90) represent the force degrees of freedom of the element. The IFM/ANALYZERS retains the same element name for different analysis methods, such as IFM, IFMD or the stiffness method. The analysis method is specified through executive control keywords such as IFM!, IFMD!, or STIFF! for primal, dual, or stiffness analysis, respectively.

The solution of a cantilevered beam, earlier used for animation as in example 2, using the IFM/ANALYZERS (HX20\_90 element) as well as MSC/NASTRAN analyzer (twenty-node CHEXA element), are given here for the purpose of illustration. The beam geometry and discretizations are depicted in figure 3. The cantilever beam is subjected to a concentrated load of 10 lb which is distributed among the eight nodes at its free end. Results obtained for two models (a three-element model and a six-element model) are depicted in table VII. The closed form strength of material solution for the beam is as follows:

Maximum displacement:  $\delta_{tip} = 2.304 \times 10^{-3}$  in.  
 Maximum stress:  $\sigma_{sup} = 720$  psi  
 Fundamental frequency:  $f = 224.3$  Hz

The tip displacement and frequency given by the strength of material formulae are quite accurate. However, stresses obtained by the beam formula and three-dimensional elasticity analysis can differ for the problem because of boundary restraints and the participation of Poisson’s ratio.

For this problem, the tip displacement for three- and six-element models obtained by IFM/IFMD, the stiffness method,

TABLE VI.—ELEMENT LIBRARY FOR IFM/ANALYZERS

Element name	Description	Degrees of freedom (fof)	Degrees of freedom (dof)
HX08_18	Hexahedral solid element with 8 nodes	18	24
HX08_33		33	24
HX08_48		48	24
HX20_57	Hexahedral solid element with 20 nodes	57	60
HX20_60		60	60
HX20_90		90	60
TH04_06	Tetrahedral solid element with 4 nodes	6	12
TH04_18		18	12
TH04_21		21	12
TH10_36	Tetrahedral solid element with 10 nodes	36	30
TH10_39		39	30
TH10_48		48	30
QD04_05	Quadrilateral membrane element with 4 nodes	5	12
QD04_07		7	12
QD04_12		12	12
QD08_13	Quadrilateral membrane element with 8 nodes	13	24
QD08_15		15	24
QD08_18		18	24
TR03_03	Triangular membrane element with 3 nodes	3	9
TR03_05		5	9
TR03_07		7	9
TR06_09	Triangular membrane element with 6 nodes	9	18
TR06_11		11	18
TR06_12		12	18
TS02_01	Truss membrane element with 2 nodes	1	6

TABLE VII.— ANALYSIS OF A CANTILEVER BEAM

Model	IFM/IFMD			Stiffness method		MSC/NASTRAN		
	Maximum von-Mises stress, psi	Maximum displacement in $10^{-3}$ in.	Frequency in Hz, (1st mode)	Maximum displacement in $10^{-3}$ in.	Frequency in Hz, (1st mode)	Maximum von-Mises stress, psi	Maximum displacement in $10^{-3}$ in.	Frequency in Hz, (1st mode)
Six/HX20_90	629.7	2.270	226.339	2.245	228.031	355.9	2.250	228.031
Three/HX20_90	573.553	2.214	230.549	2.161	234.049	348.9	2.486	234.049

and MSC/NASTRAN agreed well with an error of about 1.475, 2.56 and 2.343 percents, respectively. Fundamental frequency obtained by the three different analyzers also agreed within one-percent error. There is a remarkable difference in stress field accuracy between the force and displacement method analyzers. IFM/ANALYZERS stress converged to 629.7 psi whereas MSC/NASTRAN provided a value of 355.9 psi for the six HX20\_90 elements model. Stresses by IFM/ANALYZERS improved to 690 psi (corresponding to a 0.2 percent accuracy) at a location 0.5 in. away from the restrained nodes when an irregular model with seven elements was used. The von-Mises stress contours obtained by IFM/ANALYZERS are depicted in figure 11(a) and those obtained by MSC/NASTRAN are depicted in figure 11(b). From figure 11, we observe the following:

- (1) The neutral plane is well identified by both IFM and MSC/NASTRAN analyzers.
- (2) The stress patterns by IFM/IFMD and MSC/NASTRAN also look similar along the entire volume of the beam.
- (3) The peak stress value depicted by MSC/NASTRAN is only 56.5 percent that of IFM/ANALYZERS.
- (4) Only IFM/IFMD analyzers produce accurate stresses. Stresses predicted by MSC/NASTRAN are too low.

All the analyzers (IFM/IFMD, stiffness, and MSC/NASTRAN) can provide acceptable values for displacements and frequencies. Stress accuracy is different between IFM/ANALYZERS and MSC/NASTRAN analyzers. Only the IFM/ANALYZERS can provide accurate stresses in addition to correct displacements and frequencies.

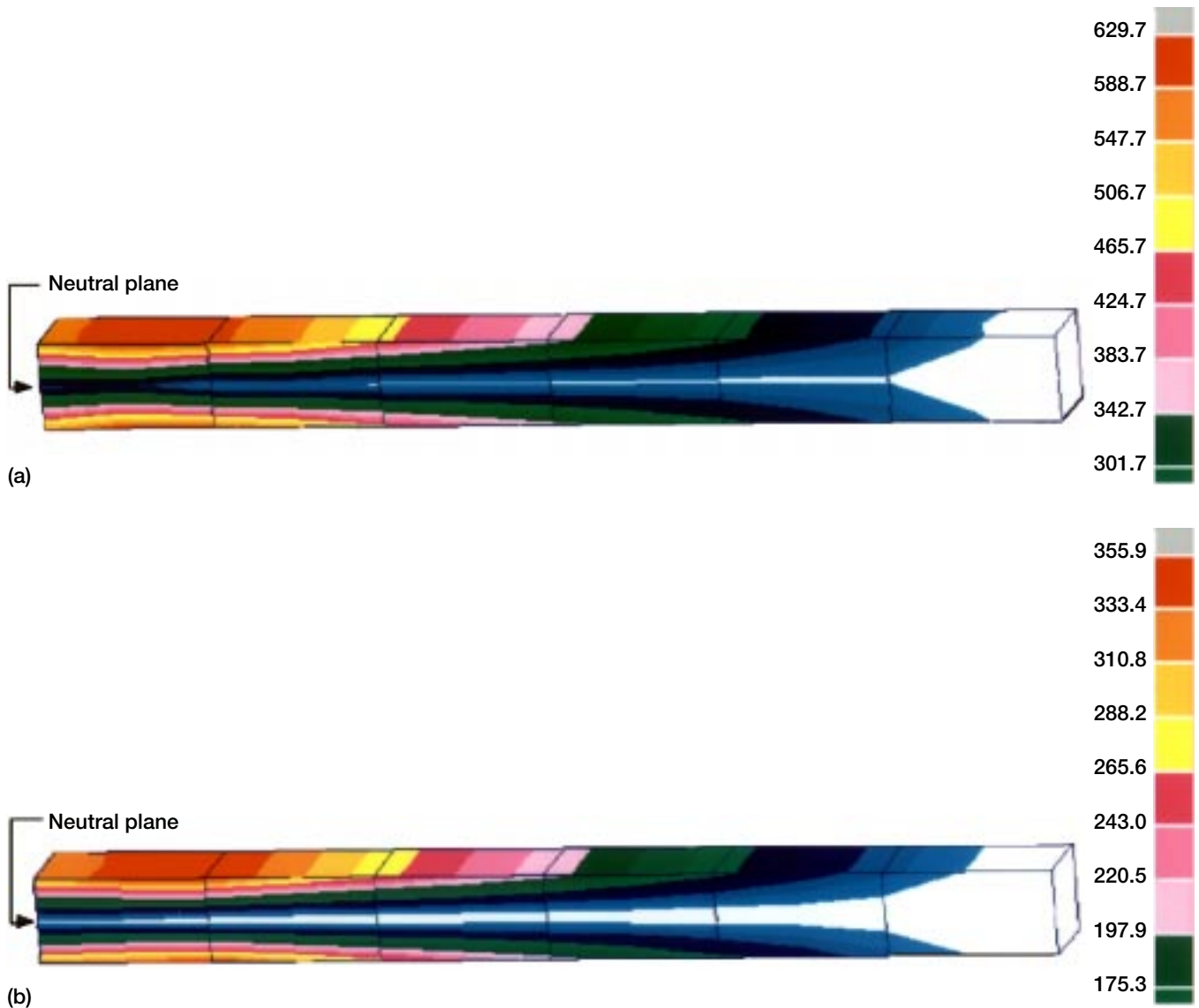


Figure 11.—Von\_Mises stresses for a cantilevered beam. (a) IFM/ANALYZERS: maximum  $\sigma_{\text{von}_M} = 629.7$  psi with six HX20\_90 elements. (b) MSC/NASTRAN analyzer: maximum  $\sigma_{\text{von}_M} = 355.9$  psi with six twenty-node CHEXA elements.

## References

1. MSC/NASTRAN Quick Reference Guide, Ver. 68, MacNeal-Schwendler Corporation, Los Angeles, CA, 1994.
2. P3/PATRAN User Manual, Publication No. 903000, vol. 3, PDA Engineering, Patran Division, Costa Mesa, CA, 1993.
3. Argyris, J.H.: ASKA-Automatic System for Kinematic Analysis—A Universal System for Structural Analysis Based on the Matrix Displacement/Finite Element Method. Nucl. Eng. Des., vol. 10, Aug. 1969, pp. 441–455.
4. ANSYS User's Manual, Swanson Analysis Systems, Inc., Houston, PA, 1994.
5. ABAQUS Theory Manual, Hibbitt, Karlsson & Sorensen, Inc., Providence, RI, 1993.
6. Patnaik, S.N.; L. Berke, L.; and Gallagher, R.H.: Integrated Force Method Versus Displacement Method for Finite Element Analysis. NASA TP-2937, 1990.
7. Patnaik, S.N.; Hopkins, D.A.; Aiello, R.A.; Berke, L.: Improved Accuracy for Finite Element Structural Analysis Via a New Integrated Force Method. NASA TP-3204, 1992.
8. Patnaik, S.N.; Yadagiri, S.: Frequency Analysis of Structures By Integrated Force Method, J. of Sound Vib., vol. 83, July 1982, pp. 93–109.
9. Patnaik, S.N.; Hopkins, D.A.; and Coroneos, R.M.: Structural Optimization with Approximate Sensitivities, Comput. Struct. vol 58, no. 2, Jan, 1996, pp. 407–418 (NASA TM-4553).
10. Patnaik, S.N.; and Gallagher, R.H.: Gradients of Behavior Constraints and Reanalysis Via the Integrated Force Method For Structural Analysis. Int. J. Numer. Methods Eng., vol. 23, Dec, 1986, pp. 2205–2212.
11. Patnaik, S.N.; Berke, L.; and Gallagher, R.H.: Compatibility Conditions of Structural Mechanics for Finite Element Analysis, AIAA Journal, vol.29, May, 1991, pp. 820–829.
12. Patnaik, S.N.: The Integrated Force Method Versus the Standard Force Method. Comput. Struct., vol. 22, no. 2, 1986, pp. 151–163.
13. Anderson, E. et al.: LAPACK Users' Guide. Second ed. Society for Industrial and Applied Mathematics, Philadelphia, PA, 1995.
14. HARWELL Subroutine Library Specifications, Harwell Laboratory, Oxfordshire, England, 1990.
15. Third U.S. National Congress on Computational Mechanics. Abstracts. Texas A & M University, College Station, TX, 1995.
16. Patnaik, S.N.; Guptill, J.D.; and Berke, L.: Merits and Limitations of Optimality Criteria Method for Structural Optimization, NASA TP-3373, 1993.
17. Guptill, J.D.; Coroneos, R.M.; Patnaik, S.N.; Hopkins, D.A.; and Berke, L.: CometBoards Users Manual, NASA TM-4537, 1996.
18. Gendy, A.S.; Patnaik, S.N.; Hopkins, D.A.; and Berke, L.: "Optimization of Space Station Components Using Code CometBoards", Int. J. of Computers Methods in Applied Mechanics and Engineering, vol. 129 (1996) pp. 133–149.
19. Patnaik, S.N.: Variational Energy Formulation for the Integrated Force Method. AIAA Journal, vol. 24, 1986, pp. 129–137.
20. Patnaik, S.N.; Kaljevic, I.; Hopkins, D.A.; and Saigal, S.: "Completed Beltrami-Michell Formulation for Analyzing Mixed Boundary Value Problems in Elasticity", AIAA Journal, vol. 34, no. 1, 1996, pp.143–148.

# REPORT DOCUMENTATION PAGE

*Form Approved*  
OMB No. 0704-0188

Public reporting burden for this collection of information is estimated to average 1 hour per response, including the time for reviewing instructions, searching existing data sources, gathering and maintaining the data needed, and completing and reviewing the collection of information. Send comments regarding this burden estimate or any other aspect of this collection of information, including suggestions for reducing this burden, to Washington Headquarters Services, Directorate for Information Operations and Reports, 1215 Jefferson Davis Highway, Suite 1204, Arlington, VA 22202-4302, and to the Office of Management and Budget, Paperwork Reduction Project (0704-0188), Washington, DC 20503.

<b>1. AGENCY USE ONLY</b> ( <i>Leave blank</i> )	<b>2. REPORT DATE</b> April 1997	<b>3. REPORT TYPE AND DATES COVERED</b> Technical Memorandum	
<b>4. TITLE AND SUBTITLE</b>  Dynamic Analysis With Stress Mode Animation by the Integrated Force Method		<b>5. FUNDING NUMBERS</b>  WU-505-63-5B	
<b>6. AUTHOR(S)</b>  Surya N. Patnaik, Rula M. Coroneos, and Dale A. Hopkins			
<b>7. PERFORMING ORGANIZATION NAME(S) AND ADDRESS(ES)</b>  National Aeronautics and Space Administration Lewis Research Center Cleveland, Ohio 44135-3191		<b>8. PERFORMING ORGANIZATION REPORT NUMBER</b>  E-10077	
<b>9. SPONSORING/MONITORING AGENCY NAME(S) AND ADDRESS(ES)</b>  National Aeronautics and Space Administration Washington, DC 20546-0001		<b>10. SPONSORING/MONITORING AGENCY REPORT NUMBER</b>  NASA TM-4729	
<b>11. SUPPLEMENTARY NOTES</b>  Responsible person, Rula M. Coroneos, organization code 1470, (216) 433-5205.			
<b>12a. DISTRIBUTION/AVAILABILITY STATEMENT</b>  Unclassified - Unlimited Subject Category 39  This publication is available from the NASA Center for Aerospace Information, (301) 621-0390.		<b>12b. DISTRIBUTION CODE</b>	
<b>13. ABSTRACT</b> ( <i>Maximum 200 words</i> )  Dynamic animation of stresses and displacements, which complement each other, can be a useful tool in the analysis and design of structural components. At the present time only displacement-mode animation is available through the popular stiffness formulation. This paper attempts to complete this valuable visualization tool by augmenting stress mode animation to the existing art. The reformulated method of forces, which in the literature is known as the integrated force method (IFM), became the analyzer of choice for the development of stress mode animation because stresses are the primary unknowns of its dynamic analysis. Animation of stresses and displacements, which have been developed successfully through the IFM analyzers, is illustrated in several examples along with a brief introduction to IFM dynamic analysis. The usefulness of animation in design optimization is illustrated considering the spacer structure component of the International Space Station as an example. An overview of the integrated force method analysis code (IFM/ANALYZERS) is provided in the appendix.			
<b>14. SUBJECT TERMS</b>  Integrated force method; Dynamic analysis and animation; Stress mode shapes		<b>15. NUMBER OF PAGES</b> 20	
		<b>16. PRICE CODE</b> A03	
<b>17. SECURITY CLASSIFICATION OF REPORT</b> Unclassified	<b>18. SECURITY CLASSIFICATION OF THIS PAGE</b> Unclassified	<b>19. SECURITY CLASSIFICATION OF ABSTRACT</b> Unclassified	<b>20. LIMITATION OF ABSTRACT</b>